RSC Advances

PAPER

View Article Online
View Journal | View Issue

Cite this: *RSC Adv.*, 2018, **8**, 11725

Novel Eu^{2+}-activated thiogallate phosphors for white LED applications: structural and spectroscopic analysis†

Szu-Ping Lee,[a] Ting-Shan Chan,[b] Somrita Dutta[a] and Teng-Ming Chen *[a]

Received 5th February 2018
Accepted 19th March 2018

DOI: 10.1039/c8ra01113c

rsc.li/rsc-advances

Novel Eu^{2+}-activated $BaGa_2SiS_6$ and $Ba_2Ga_8SiS_{16}$ thiogallate phosphors were prepared by solid-state reaction route. The $BaGa_2SiS_6$:Eu^{2+} phosphor generated a green emission upon excitation at 405 nm, whereas the $Ba_2Ga_8SiS_{16}$:xEu^{2+} phosphor could be tuned from cyan to green range with increasing Eu^{2+} concentration upon excitation at 365 nm. Additionally, the thermal luminescence properties of the thiogallate phosphors were investigated in the temperature range of 25 to 250 °C. A warm-white LED is fabricated using the combination of a 405 nm blue InGaN-based LED chip with the green-emitting $BaGa_2SiS_6$:$0.01Eu^{2+}$ phosphor, and red-emitting $Sr_2Si_5N_8$:Eu^{2+} commercial phosphor with the CRI value of ~88 and the CCT of 4213 K.

1. Introduction

Phosphor-converted white light emitting diodes (PC-WLEDs) have emerged as one of the most promising and eco-friendly white-light sources for general illumination, consuming less energy than conventional incandescent light sources[1–6]. In most commercial WLEDs, a combination of a blue LED chip and cerium doped yttrium aluminum garnet (YAG:Ce^{3+}) phosphor is used for the generation of white light.[7] But this combination has the shortcomings of poor colour rendering index (CRI) and a high correlated colour temperature (CCT) due to the absence of emission in the red spectral region which restricts its use in commercial lighting.[8,9] There are several approaches considered for achieving high CRI and cool color correlated temperature such as; a combination of a blue LED chip with a yellow-emitting and a narrow-band red-emitting phosphor or a mixture of green-emitting and red-emitting phosphor.[8–12] The use of a near-ultraviolet (n-UV) LED chip or an ultraviolet (UV) LED chip when combined with a mixture of red, green and blue phosphors can also improve the CRI value and the CCT values of the white light generated.[13–15] Hence there is a need to develop new phosphors for obtaining the optimal requirements for a high-quality white light for general commercial lighting applications.

One of the main approaches involved in the designing of new phosphors includes the exploration of host compounds from existing structural model and then the proper selection of suitable activators (such as broadband emitting Eu^{2+}, Ce^{3+}, and Mn^{2+}).[16] Two such hosts that can be considered for exploration are $BaGa_2SiS_6$ reported by Yin *et al.* in 2012 (ref. 17) and $Ba_2Ga_8SiS_{16}$ reported by Liu and group in the year 2014 (ref. 18) for the first time. Both the materials were studied for high power IR – nonlinear optical applications. Since, sulphide-containing lattices when activated by Eu^{2+} provide a longer emission wavelength due to their higher nephelauxetic effect compared to nitrides and oxides,[19–21] the structural design of these two materials opens up the possibility to study them for LED applications. The gallium (Ga^{3+}) and silicon (Si^{4+}) ions can create a protective environment to successfully enhance the stability of the sulfide phosphors and hence their luminescence properties.

When doped with Eu^{2+}, the emission spectrum is in general characterized by a single broad band emission which can be deconvoluted into two or more number of emission bands depending on the number of cationic sites replaced by Eu which can also help in achieving higher CRI values for WLED applications. Also, due to the small Stokes shift value, the phosphors could be excited from UV to blue region. The covalency and the crystal field splitting between the host allows Eu^{2+} ions to exhibit the parity-allowed $5d^14f^{n-1} \rightarrow 4f^n$ emission from the UV region to the visible spectral region.[22–26] In this research, a green-emitting Eu^{2+}-activated $BaGa_2SiS_6$ and a tunable cyan-to-green-emitting $Ba_2Ga_8SiS_{16}$:Eu^{2+} phosphors were reported which show broad excitation range. The structural and luminescent properties of the phosphors were investigated in detail. In addition, a LED device using the $BaGa_2SiS_6$:Eu^{2+} phosphor with a 405 nm LED chip was fabricated to demonstrate its applicability as a colour-conversion phosphor in the fabrication of WLEDs.

[a]*Phosphors Research Laboratory, Department of Applied Chemistry, National Chiao Tung University, Hsinchu 30010, Taiwan. E-mail: tmchen@mail.nctu.edu.tw*

[b]*National Synchrotron Radiation Research Center, Hsinchu 30076, Taiwan*

† Electronic supplementary information (ESI) available. See DOI: 10.1039/c8ra01113c

2. Experimental

2.1 Materials and synthesis

The Eu^{2+} -doped $BaGa_2SiS_6$ and $Ba_2Ga_8SiS_{16}$ phosphors were synthesized using BaS (Alfa Aesar, 99.7%), Ga_2S_3 (Alfa Aesar, 99.99%), Si powder (Alfa Aesar, 99.999%), and S powder (Acros, 99.999%) and EuF_2 (Alfa Aesar, 99.9%) as raw ingredients. The ingredients were homogeneously mixed and ground in a glove box under nitrogen atmosphere and loaded into the quartz glass ampoules, which were then sealed off after evacuated to 10^{-4} torr. The ampoules were heated in a furnace to 900 °C for 8 h at 5 °C min^{-1}. Finally, the powdered phosphors were obtained after the furnace naturally cooled down to room temperature. In each case, the reactions are summarized in the following equations.

$$(1-x)BaS + Ga_2S_3 + xEuF_2 + Si + 2S \rightarrow (Ba_{1-x}Eu_x)Ga_2SiS_6 \quad (1)$$

$$(2-2x)BaS + 4Ga_2S_3 + 2xEuF_2 + 2Si + 4S \rightarrow (Ba_{1-x}Eu_x)_2Ga_8SiS_{16} + SiS_2\uparrow \quad (2)$$

2.2 Characterizations

Synchrotron X-ray Diffraction (SXRD) using the BL01C2 beamline with an X-ray wavelength of 0.774908 Å was used to analyse the phase purity of the synthesized products by at the National Synchrotron Radiation Research Centre (NSRRC) in Hsinchu, Taiwan. The X-ray Rietveld refinement was carried to investigate the structure of the phosphor using the General Structure Analysis System (GSAS) software. JEOL JSM-7401F operated at voltage of 5 kV was used to perform the scanning electron microscopy (SEM) morphological analysis and energy dispersive X-ray spectroscopy (EDS) analysis. The photoluminescence spectra and the time resolved measurement of the phosphors were obtained using a FS5 Fluorescence Spectrometer (Edinburgh Instruments) with a 450 W xenon lamp and a TCSPC (Time Correlated Single Photon Counting) module in combination with EPLED-360 picosecond pulsed light emitting diode laser system as the excitation source respectively. An integrating sphere whose inner face was coated with Spectralon equipped with a spectrofluorometer (Horiba Jobin-Yvon Fluorolog 3-2-2) measured the quantum efficiency (QE). The thermal luminescence performance was analyzed using a heating apparatus (THMS-600) fitted with PL equipment. The electroluminescence (EL) spectra were performed by Sphere-Optics integrating sphere with LED measurement starter packages (Onset, Inc.) recording at different current in the range of 100–300 mA.

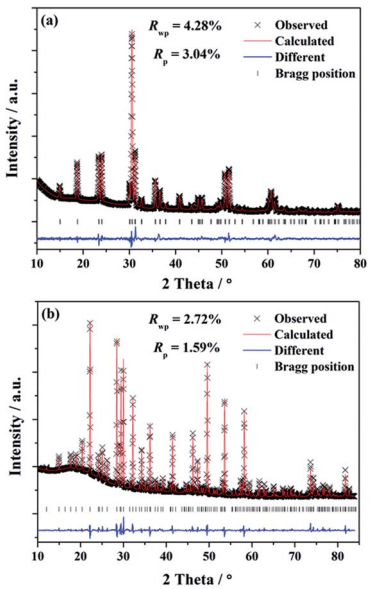

Fig. 1 The SXRD profiles for Rietveld refinement results of (a) $(Ba_{0.95}Eu_{0.05})Ga_2SiS_6$ and (b) $(Ba_{0.90}Eu_{0.10})_2Ga_8SiS_{16}$. Observed intensities (cross), calculated patterns (red line), Bragg positions (tick mark), and difference plot (blue line) are presented.

Table 1 Structural parameters of $(Ba_{0.95}Eu_{0.05})Ga_2SiS_6$ and $(Ba_{0.90}Eu_{0.10})_2Ga_8SiS_{16}$ of Rietveld Refinement from SXRD data at room temperature[a]

Formula	$(Ba_{0.95}Eu_{0.05})Ga_2SiS_6$	$(Ba_{0.90}Eu_{0.10})_2Ga_8SiS_{16}$
Symmetry	Trigonal	Hexagonal
Space group	*R*3 (no. 146)	$P6_3mc$ (no. 186)
Lattice parameters	$a = b = 9.55032(28)$	$a = b = 10.83380(10)$
	$c = 8.63634(27)$	$c = 11.86626(18)$
	$V = 682.18(4)$	$V = 1206.164(25)$
R_{wp}	4.28%	4.68%
R_p	3.04%	2.75%
χ^2	3.805	2.873

[a] Lattice parameters: *a* and *c* in Å, *V* in $Å^3$; $T = 298$ K; BL01C2 beamline of NSRRC, $\lambda = 0.774908$ Å; Site Occupancy Fraction (S.O.F.); U_{iso} in $Å^2$.

$(Ba_{0.95}Eu_{0.05})Ga_2SiS_6$

Atom	*x*/*a*	*y*/*b*	*z*/*c*	S.O.F	U_{iso}*100
Ba	0.00000	0.000000	0.4988(26)	0.9500	6.59
Ga	0.0537(13)	0.8276(10)	0.9498(29)	0.6700	0.30
Si	0.049351	0.7379(22)	0.8921(74)	0.3300	1.34
S(1)	0.8527(13)	0.5886(12)	0.5146(28)	1.0000	3.12
S(2)	0.8136(15)	0.7627(13)	0.8284(27)	1.0000	1.63
Eu	0.000000	0.000000	0.4988(26)	0.0500	6.59

$(Ba_{0.90}Eu_{0.10})_2Ga_8SiS_{16}$

Atom	*x*/*a*	*y*/*b*	*z*/*c*	S.O.F	U_{iso}*100
Ba(1)	0.333300	0.666700	0.0253(8)	0.9500	4.53
Ba(2)	0.333300	0.666700	0.5156(8)	0.9500	2.59
Ga(1)	0.0048(17)	0.3384(11)	0.3262(65)	0.8600	1.42
Ga(2)	0.8846(5)	0.1154(5)	0.0746(13)	1.0000	2.16
Si	0.0048(17)	0.3384(11)	0.3262(65)	0.1400	1.42
S(1)	0.6625(14)	0.0040(14)	0.0164(7)	1.0000	1.72
S(2)	0.2255(11)	0.7745(11)	0.2637(18)	1.0000	1.06
S(3)	0.5593(9)	0.4407(9)	0.2791(20)	1.0000	1.61
S(4)	0.8977(11)	0.1023(11)	0.2664(18)	1.0000	0.53
S(5)	1.000000	0.000000	−0.0162(22)	1.0000	2.70
Eu(1)	0.333300	0.666700	0.0253(8)	0.0500	4.53
Eu(2)	0.333300	0.666700	0.5156(8)	0.0500	2.59

Table 2 Selected interatomic bond distances[a] of $(Ba_{0.95}Eu_{0.05})Ga_2SiS_6$ and $(Ba_{0.90}Eu_{0.10})_2Ga_8SiS_{16}$ at room temperature

$(Ba_{0.95}Eu_{0.05})Ga_2SiS_6$		$(Ba_{0.90}Eu_{0.10})_2Ga_8SiS_{16}$	
(Ba/Eu)-S1	3.45104(10) (3×)	(Ba1/Eu1)-S1	3.61231(3) (6×)
(Ba/Eu)-S1^i	3.50580(8) (3×)	(Ba1/Eu1)-S2	3.47936(4) (3×)
(Ba/Eu)-S2	3.51719(8) (3×)	(Ba1/Eu1)-S3	3.54776(4) (3×)
(Ba/Eu)-S2^i	3.60984(11) (3×)	(Ba2/Eu2)-S1	3.54578(3) (6×)
Ga-S1	2.27107(7)	(Ba2/Eu1)-S2	3.60961(4) (3×)
Ga-S1^i	2.40444(7)	(Ba2/Eu1)-S3	3.71969(4) (6×)
Ga-S2	2.20099(6)	(Ga1/Si)-S1	2.25675(3)
Ga-S2^i	2.12290(5)	(Ga1/Si)-S2	2.19921(2)
		(Ga1/Si)-S3	2.19370(2)
		(Ga1/Si)-S4	2.32944(2)
		Ga2-S1	2.19539(2) (2×)
		Ga2-S4	2.28965(3)
		Ga2-S5	2.41845(2)

[a] Bond distance in Å.

3. Results and discussion

3.1 Structural characterizations and crystallographic parameters of the $(Ba_{0.95}Eu_{0.05})Ga_2SiS_6$ and $(Ba_{0.90}Eu_{0.10})_2Ga_8SiS_{16}$ phosphors

To investigate the phases of the obtained phosphors and a knowledge of their crystal structure, the Rietveld analysis[22] was performed using the single crystal structure data of $BaGa_2SiS_6$ (ICSD file no. 184747) and $Ba_2Ga_8SiS_{16}$ (ICSD file no. 194875), respectively, as references to approach a dependable approximation of the actual crystal structure. The experimental, calculated, and structural results of the SXRD refinement of $(Ba_{0.95}Eu_{0.05})Ga_2SiS_6$ and $(Ba_{0.90}Eu_{0.10})_2Ga_8SiS_{16}$ are shown in Fig. 1a and b, respectively.

The final refinement converged with weighted-profiles of $R_p = 3.04\%$ and $R_{wp} = 4.28\%$ of $(Ba_{0.95}Eu_{0.05})Ga_2SiS_6$; $R_p = 1.59\%$ and $R_{wp} = 2.72\%$ of $(Ba_{0.90}Eu_{0.10})_2Ga_8SiS_{16}$, thus revealing the good quality of the refinement. The crystallographic data are summarized and the selected bond lengths are available in Table 1 and 2, respectively.

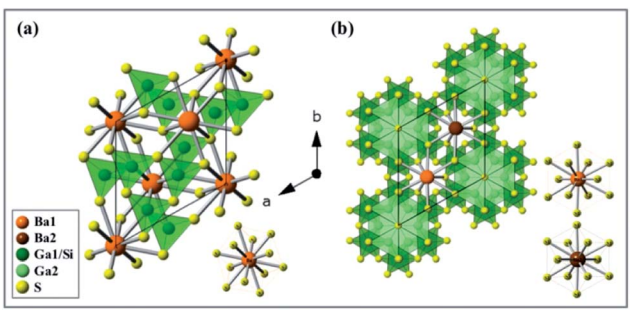

Fig. 2 (a) Schematic crystal structure of $BaGa_2SiS_6$ (trigonal, $R3$) (a) and $Ba_2Ga_8SiS_{16}$ (hexagonal, $P6_3mc$) (b) viewed down the c-axis. Orange, brown, green, light green and yellow sphere balls describe Ba1, Ba2, Ga1/Si, Ga2, S and Si atoms. The insets show the coordination environment around BaS_{12} (left-down) of $BaGa_2SiS_6$, $Ba1S_{12}$ (right-up) and $Ba2S_{12}$ (right-down) of $Ba_2Ga_8SiS_{16}$.

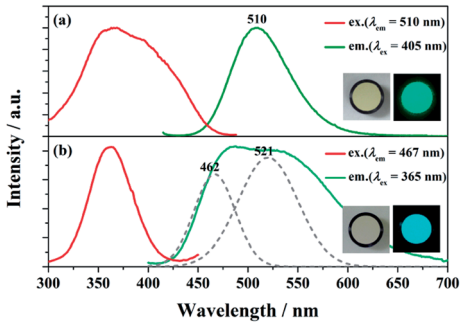

Fig. 3 (a) PLE/PL spectra of $BaGa_2SiS_6$:0.01Eu^{2+}. (b) PLE/PL spectra and the PL deconvolution (dashed line) of $Ba_2Ga_8SiS_{16}$:0.01Eu^{2+}. The insets show photos of the phosphor taken under normal light (left) and 365 nm UV light (right).

The as-synthesized $BaGa_2SiS_6$ phosphor was found to crystallize in the space group $R3$ of the trigonal system, whereas the $Ba_2Ga_8SiS_{16}$ in the space group $P6_3mc$ of the hexagonal system. Fig. 2a presents the exact crystal structure of $BaGa_2SiS_6$ viewed along the c-axis and a single Ba atomic site (BaS_{12}). Fig. 2b indicates the crystal structure of $Ba_2Ga_8SiS_{16}$, which shows two crystallographically-independent Ba atomic sites (Ba1 and Ba2) along with the Ga/SiS_4 tetrahedral coordination.

The grain size and morphology of the two phosphor particles characterized by SEM show that the as-synthesized phosphor was composed of irregular granular micro crystals. The nominal stoichiometry was also verified by EDS measurement, as shown in Fig. S1.†

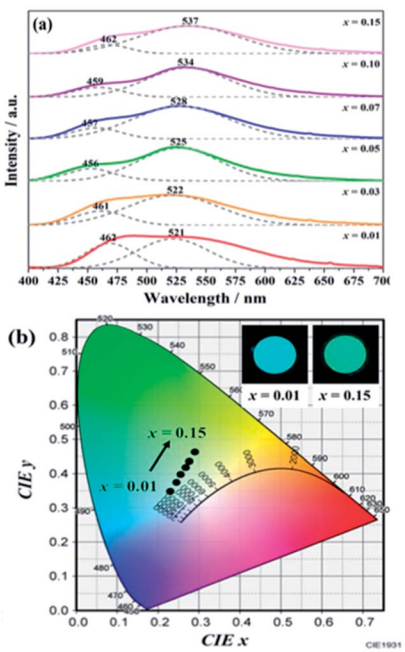

Fig. 4 PL spectra (a) and variation in CIE chromaticity coordinates (b) of $(Ba_{1-x}Eu_x)_2Ga_8SiS_{16}$ ($0.01 \leq x \leq 0.15$) phosphor as a function of Eu^{2+} content.

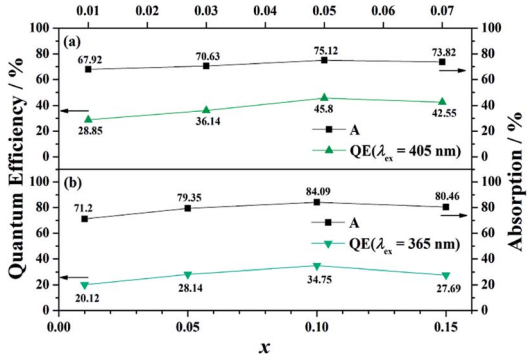

Fig. 5 Absorption (A) and external quantum efficiency (EQE) as a function of x in $(Ba_{1-x}Eu_x)Ga_2SiS_6$ ($0.01 \leq x \leq 0.10$) and $(Ba_{1-x}Eu_x)_2Ga_8SiS_{16}$ ($0.01 \leq x \leq 0.15$) under excitation at 405 and 365 nm, respectively.

3.2 Spectroscopic study of the $BaGa_2SiS_6:Eu^{2+}$ and $Ba_2Ga_8SiS_{16}:Eu^{2+}$ phosphor

The PLE and PL spectra of $BaGa_2SiS_6:0.01Eu^{2+}$ and $Ba_2Ga_8SiS_{16}:0.01Eu^{2+}$ is represented in Fig. 3. The $BaGa_2SiS_6:Eu^{2+}$ phosphor is excitable around 350 to 450 nm and generates a green emission peaking at 510 nm, and the $Ba_2Ga_8SiS_{16}:Eu^{2+}$ phosphor exhibits a broadband cyan emission upon excitation at 365 nm. The two emission bands of $Ba_2Ga_8SiS_{16}:Eu^{2+}$ are attributed to the two sites of barium atom (Ba1 and Ba2) in the $Ba_2Ga_8SiS_{16}$ lattice.

As indicted in Fig. 4, the Eu^{2+} emission peak changes from 462 and 521 nm (1% Eu^{2+}) to 462 and 537 nm (15% Eu^{2+}) with the increasing Eu^{2+} concentration. In addition, the intensity of the short emission decreases while that of the long emission enhances as Eu^{2+} concentration increases. This may result from the fact that Eu^{2+} occupy in different sites, *viz*, Ba1 and Ba2 sites in the $Ba_2Ga_8SiS_{16}$ lattice, and the energy transfer between Eu^{2+} ions in the two different sites occur with increasing Eu^{2+} concentration.

Moreover, $BaGa_2SiS_6:Eu^{2+}$ exhibits a higher external quantum efficiency (EQE) values than that of $Ba_2Ga_8SiS_{16}:Eu^{2+}$ (Fig. 5). The comparatively high asymmetry in $BaGa_2SiS_6:Eu^{2+}$ crystal may be the major reason for the higher EQE. With an increase in absorption, the EQE value for $(Ba_{1-x}Eu_x)Ga_2SiS_6$ ($0.01 \leq x \leq 0.10$) increases and reaches maximum values of about 45.80% at $x = 0.10$, whereas $(Ba_{1-x}Eu_x)_2Ga_8SiS_{16}$ ($0.01 \leq x \leq 0.15$) reaches maximum values of about 34.75% at $x = 0.10$, as shown in Fig. 5.

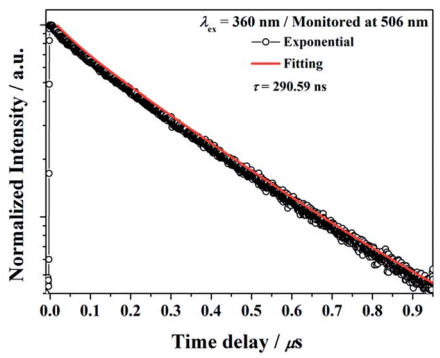

Fig. 6 Decay curve for $BaGa_2SiS_6:Eu^{2+}$ phosphor (black line) and curve-fitting (red line) under 360 nm excitation and monitored at 506 nm.

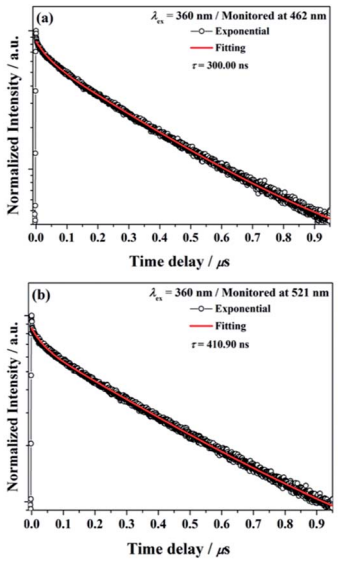

Fig. 7 Decay curve for $Ba_2Ga_8SiS_{16}:Eu^{2+}$ phosphor (black line) and curve-fitting (red line) under 360 nm excitation and monitored at (a) 462 nm and (b) 521 nm.

3.3 Time resolved measurement and thermal luminescence properties of the $BaGa_2SiS_6:Eu^{2+}$ and $Ba_2Ga_8SiS_{16}:Eu^{2+}$ phosphor

The decay curve of $BaGa_2SiS_6:Eu^{2+}$ phosphor excited at 360 nm and monitored at 506 nm is presented in Fig. 6. The measured lifetime is related to the first-order exponential equation given by[27]

$$I = I_0 \exp\left(\frac{-t}{\tau}\right)$$

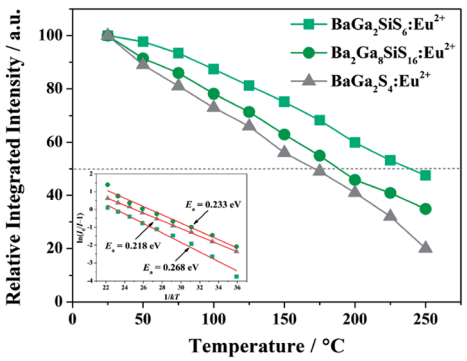

Fig. 8 Temperature dependence of relative PL integrated intensity for $BaGa_2SiS_6:Eu^{2+}$, $Ba_2Ga_8SiS_{16}:Eu^{2+}$, and $BaGa_2S_4:Eu^{2+}$ over the range 25 to 250 °C. The inset shows the fitted PL integrated intensity and the calculated thermal activation energy (E_a) as a function of temperature.

The luminescence decay times τ was calculated to be 290.59 ns for $BaGa_2SiS_6:Eu^{2+}$, the result is acceptable for the parity-allowed $4f^65d^1 \rightarrow 4f^7$ transitions of Eu^{2+} and rapid enough for LED lighting applications. Moreover, the well-fitting results by an exponential decay with a single component illustrate that Eu^{2+} ions occupy only one site in the $BaGa_2SiS_6$ host.

The decay curves of $Ba_2Ga_8SiS16:Eu^{2+}$ phosphor monitored at 462 nm ($\tau = 300.00$ ns) and monitored at 521 nm ($\tau = 410.90$ ns) under 360 nm excitation are illustrated in Fig. 7a and b, respectively. The results indicated that the Eu^{2+} ions occupied the two different Ba^{2+} ions coordination environment in the $Ba_2Ga_8SiS_{16}$ host.

Both thiosilicate phosphors were found to remain intact when left in the air at ambient temperature for 10–14 days with 60–70% relative humidity. Thermal luminescence quenching property of a phosphor plays an important role for LED applications. Fig. 8 shows temperature dependence of relative PL integrated intensity for $BaGa_2SiS_6:Eu^{2+}$, $Ba_2Ga_8SiS_{16}:Eu^{2+}$, and $BaGa_2S_4:Eu^{2+}$ over the range 25 to 250 °C. The thermal stability of the as-prepared thiogallate phosphors is stronger than that of the ternary sulfide $BaGa_2S_4:Eu^{2+}$, which perhaps belongs to the stiff (SiS_4) tetrahedral network that makes the host more stable. The lower left inset of Fig. 8 presents the calculated thermal activation energy (E_a) expressed by the following equation:[28]

$$I(T) = \frac{I_0}{1 + A\exp\left(-\frac{E_a}{kT}\right)} \quad (3)$$

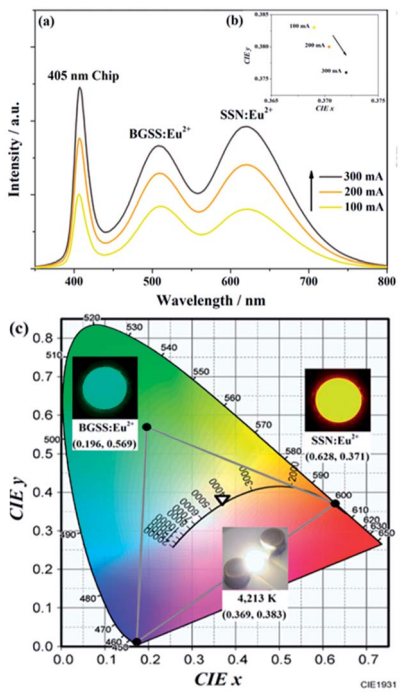

Fig. 9 (a) EL spectra of the device using 405 nm LED chip with green-emitting $BaGa_2SiS_6:Eu^{2+}$ phosphor, and red-emitting $Sr_2Si_5N_8:Eu^{2+}$ phosphor and (b) variation in CIE chromaticity coordinates of the WLED operated under different currents (100 to 300 mA). (c) CIE chromaticity coordinates of the used phosphors and the fabricated LED are presented. The insets show the used phosphors and the LED device photos recorded under 365 nm excitation.

where I_0 and $I(T)$ represent the PL integrated intensity at room temperature and testing temperature (25–250 °C), respectively, and k the Boltzmann constant. The values of E_a for $BaGa_2SiS_6:Eu^{2+}$, $Ba_2Ga_8SiS_{16}:Eu^{2+}$, and $BaGa_2S_4:Eu^{2+}$ were estimated to be 0.268, 0.233 and 0.218 eV, respectively.

3.4 CIE chromaticity coordinates and performance of LED devices based on $BaGa_2SiS_6:Eu^{2+}$ phosphor

To reveal the prospective use of $BaGa_2SiS_6:Eu^{2+}$ for PC-WLED application, the $BaGa_2SiS_6:0.01Eu^{2+}$ phosphor was utilized to fabricate a WLED device driven by 100 to 300 mA current with red-emitting $Sr_2Si_5N_8:Eu^{2+}$ and a 405 nm LED chip shown in Fig. 9.

The EL intensity of the blue, green, and red bands of the white LED device increased while increasing the forward-biased current from 100 to 300 mA, and the saturation phenomenon was not observed even at a high forward current of 300 mA, as illustrated in Fig. 9a. As shown in Fig. 9b, with an increase in the driving current, the CIE chromaticity coordinates shifted slightly. The results demonstrated the excellent colour stability of the $BaGa_2SiS_6:0.01Eu^{2+}$ phosphor. In Fig. 9c the studies indicate that this novel green phosphor is a potential candidate for white LED, especially for the generation of warm white light with an optimum CRI of 88 and a CCT value of 4213 K.

4. Conclusions

In summary, we have investigated two new Eu^{2+}-doped $BaGa_2SiS_6$ and $Ba_2Ga_8SiS_{16}$ thiogallate phosphors. The crystal structure and luminescence performance of both the phosphors were studies in detail. The results reveal that the green-emitting Eu^{2+}-doped $BaGa_2SiS_6$ and the colour-tunable Eu^{2+}-doped $Ba_2Ga_8SiS_{16}$ could be excited over a broad range of wavelength thus generating a broadband emission. The green-emitting Eu^{2+}-doped $BaGa_2SiS_6$ phosphor was integrated together with a red-emitting phosphor and a blue chip to obtain a warm-white-light LED device an optimum CRI value of 88 and CCT value of 4213 K. Our investigation indicates the potential use of this phosphor in phosphor-converted LED for the lighting application.

Conflicts of interest

There are no conflicts of interest to declare.

Acknowledgements

This research was financially supported by Ministry of Science and Technology of Taiwan (R.O.C.) under Contract No. MOST104-2113-M-009-018-MY3.

References

1 G. Blasse and B. C. Grabmaier, *Luminescent Materials*, Springer-Verlag, Berlin, 1994.
2 B. Damilano, P. Demolon, J. Brault, T. Huault, F. Natali and J. Massies, *J. Appl. Phys.*, 2010, **108**, 73115–73121.

3 S. Ye, F. Xiao, Y. Pan, Y. Ma and Q. Zhang, *Mater. Sci. Eng., R*, 2010, **71**, 1–34.
4 R. Mueller-Mach, G. Mueller, M. R. Krames, H. A. Hoppe, F. Stadler, W. Schnick, T. Juestel and P. Schmidt, *Phys. Status Solidi A*, 2005, **202**, 1727–1732.
5 L. Chen, C. C. Lin, C. W. Yeh and R. S. Liu, *Materials*, 2010, **3**, 2172–2195.
6 H. A. Höppe, *Angew. Chem., Int. Ed.*, 2009, **48**, 3572–3582.
7 D. J. Robbins, *J. Electrochem. Soc.*, 1979, **126**, 1550–1555.
8 H. Lin, B. Wang, J. Xu, R. Zhang, H. Chen, Y. L. Yu and Y. S. Wang, *ACS Appl. Mater. Interfaces*, 2014, **6**, 21264–21269.
9 R. J. Xie, N. Hirosaki, T. Suehiro, F. F. Xu and M. A. Mitomo, *Chem. Mater.*, 2006, **18**, 5578–5583.
10 J. H. Oh, H. Y. Kang, J. Eo, H. K. Park and Y. R. Do, *J. Mater. Chem. C*, 2015, **3**, 607–615.
11 X. Piao, K. I. Machida, T. Horikawa, H. Hanzawa, Y. Shimomura and N. Kijima, *Chem. Mater.*, 2007, **19**, 4592–4599.
12 K. A. Denault, N. C. Gerorge, S. R. Paden, S. Brinkley, A. A. Mikhailovsky, J. Neuefeind, S. P. DenBaars and R. Seshardri, *J. Mater. Chem.*, 2012, **22**, 18204–18213.
13 Z. Xia, Z. Xu, M. Chen and Q. Liu, *Dalton Trans.*, 2016, **45**(28), 11214–11232.
14 Z. Yang, P. C. Lin, C. F. Guo and W.-R. Liu, *RSC Adv.*, 2015, **5**, 13184–13191.
15 S. Dutta, S. Som and S. K. Sharma, *Dalton Trans.*, 2013, **42**, 9654–9661.
16 Z. Xia and Q. Liu, *Prog. Mater. Sci.*, 2016, **84**, 59–117.
17 W. L. Yin, K. Feng, R. He, D. J. Mei, Z. H. Lin, J. Y. Yao and Y. C. Wu, *Dalton Trans.*, 2012, **41**, 5653–5661.
18 B. W. Liu, H. Y. Zeng, M. J. Zhang, Y. H. Fan, G. C. Guo and J. S. Huang, *Inorg. Chem.*, 2015, **54**, 976–981.
19 J. E. Van Haecke, P. F. Smet and D. Poelman, *J. Lumin.*, 2007, **126**, 508–514.
20 P. F. Smet, I. Moreels, Z. Hens and D. Poelman, *Materials*, 2010, **3**, 2834–2883.
21 A. B. Parmentier, P. F. Smet and D. Poelman, *Opt. Mater.*, 2010, **33**, 141–144.
22 G. Li, Y. Tian, Y. Zhao and J. Lin, *Chem. Soc. Rev.*, 2015, **44**, 8688–8713.
23 J. Shi and S. Zhang, *J. Phys. Chem. B*, 2004, **108**, 18845–18849.
24 A. Piquette, W. Bergbauer, B. Galler and K. C. Mishra, *ECS J. Solid State Sci. Technol.*, 2016, **5**(1), R3146–R3159.
25 C.-H. Huang, Y.-C. Chen, T.-M. Chen, T.-S. Chan and H.-S. Sheu, *J. Mater. Chem.*, 2011, **21**, 5645–5649.
26 D. Y. Wang, C. H. Huang, Y. C. Wu and T. M. Chen, *J. Mater. Chem.*, 2011, **21**, 10818–10822.
27 R. Pang, C. Li, L. Shi and Q. Su, *J. Phys. Chem. Solids*, 2009, **70**, 303–306.
28 R. J. Xie, N. Hirosaki, N. Kimura, K. Sakuma and M. Mitomo, *Appl. Phys. Lett.*, 2007, **90**, 191101–191103.